

pubs.acs.org/JACS Communication

CO₂ Desorbs Water from K-MER Zeolite under Equilibrium Control

Hwangho Lee, Dan Xie, Stacey I. Zones, and Alexander Katz*



Cite This: J. Am. Chem. Soc. 2024, 146, 68–72



ACCESS

Metrics & More

Article Recommendations

SI Supporting Information

ABSTRACT: Competitive adsorption by water in zeolites is so strongly prevalent that established gravimetric techniques for quantification have assumed that humid CO_2 has no effect on preadsorbed water at the same relative humidity. Here, we demonstrate sites in small-pore zeolite K-MER, in which CO_2 adsorption causes 20% of preabsorbed water to desorb under equilibrium control at 30 °C and 5% relative humidity. Diffuse reflectance IR spectroscopic data demonstrate that dimeric water species that are coordinated to cationic sites in K-MER zeolite are selectively displaced by CO_2 under these humid conditions. Though Cs-RHO contains more weakly bound water than K-MER, we observe a lack of dimeric water species and no evidence of CO_2 outcompeting water in Cs-RHO. We conclude that the desorption of water by CO_2 in K-MER is driven by a highly desired site for CO_2 adsorption as opposed to an intrinsically weak binding of water to the zeolite. Our demonstration that CO_2 can outcompete water in a zeolite under wet conditions introduces new opportunities for the design of selective sites for humid CO_2 adsorption and stresses the importance of independently characterizing adsorbed water and CO_2 in these systems.

eolites are regarded as promising host candidates for CO₂ capture and storage (CCS) due to their high volumetric capacity, as well as the tunability afforded by their exchangeable cations and microporous framework structure, which control guest adsorption. $^{1-9}$ However, the presence of water in flue gas, unavoidable for a postcombustion gas mixture, causes competitive adsorption that has been shown to significantly diminish CO_2 adsorption. $^{10-13}$ It is essential to develop a deeper understanding of humid CO2 adsorption in zeolites, in order to enable the rational design of these functional materials, $^{5,14-17}$ particularly as new understanding emerges about the role of water under zeolitic confinement. 18,19 When characterizing humid CO₂ adsorption in Cs-RHO zeolite, we have recently demonstrated a synergistic role in which water facilitates humid CO₂ adsorption. 15 We used thermogravimetric analysis (TGA) to estimate water and CO₂ uptakes in conjunction with a long-standing heuristic, ^{5,13,20–25} which assumes that the adsorption of CO2 under wet conditions does not cause the desorption of equilibrated water at the same relative humidity.²⁶ Motivated by K-MER zeolite being investigated extensively as a host for CCS, 9,12,27-29 in this study, initially, we apply the approach above to measure the humid CO₂ uptake of K-MER (Table 1) at 5% relative humidity and 30 °C (see Figure S2 and Table \$1, Supporting Information).

Table 1. Chemical Composition of K-MER and Cs-RHO Obtained by ICP-AES Results

	Si (wt %)	Al (wt %)	Cs (wt %)	K (wt %)	Si/ Al ₂ ^a	M ⁺ /Al ^a
K-MER	22.8	11.0		15.0	4.00	0.94
Cs-RHO	21.8	5.66	27.9		7.41	0.99

^aMolar ratio.

In order to understand the interactions between CO₂ and water during humid CO₂ adsorption, we independently characterize water and CO₂ by combined diffuse-reflectance Fourier-transform infrared spectroscopy (DRIFTS) and TGA. In situ DRIFTS bands at 3800-3000 and 1640 cm⁻¹ in Figure 1a and 1b are assigned to -OH stretching and H-O-H bending vibrations of water clusters within K-MER zeolite, respectively. These data demonstrate a significant decrease in both infrared bands of water after humid CO₂ adsorption. We conclude that CO₂ adsorption leads to the desorption of preequilibrated water at 5% relative humidity (RH) in K-MER zeolite, which is also supported by TGA (see Figures S3, Supporting Information). Such desorption of equilibrated water at the same relative humidity as humid CO2 adsorption goes against conventional wisdom, which states that CO2 is unable to displace preadsorbed water in zeolites under equilibrium control. 20-25 Combining DRIFTS data of Figure 1 and TGA, we quantify the amount of desorbed water caused by humid CO₂ adsorption at 5% RH to be 1.17 mmol/g (see Figures S2, S4-S6, Supporting Information). These results indicate that CO₂ must adsorb in a greater amount compared to what is measured using TGA alone, in which the conventional approach assumes that the amount of desorbed water released during humid CO2 adsorption is zero by a heuristic.5,13 When accounting for the actual amount of desorbed water, the true humid CO2 uptake in K-MER zeolite is nearly 60% higher (1.27 mmol/g) than the 0.8 mmol/g measured with the conventional approach of TGA combined

Received: October 1, 2023
Revised: December 11, 2023
Accepted: December 12, 2023
Published: December 21, 2023





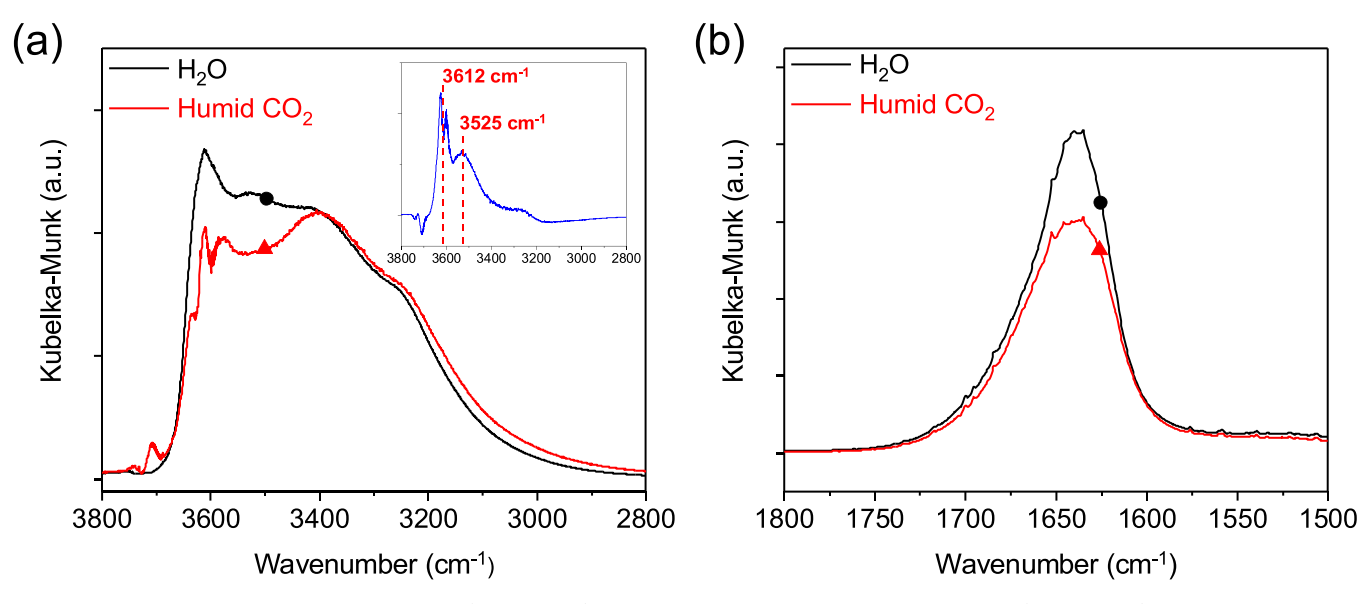


Figure 1. DRIFT spectra after water saturation (black, circle) and subsequent saturation with humid CO₂ (red, triangle) at 30 °C, both at 5% relative humidity. Spectra in the (a) OH-stretch and (b) H-O-H bending spectral regions for adsorbed water in K-MER. The inset in (a) shows the subtraction of black (circle) to red (triangle) spectra.

with the heuristic. This result emphasizes the critical importance of understanding the interactions of water and CO_2 in zeolites.

We compared the phenomena in Figure 1 with Cs-RHO as a small-pore zeolite with D8R (double eight-membered rings), which has been previously demonstrated to be effective for humid CO₂ adsorption (see Tables 1 and S1, Supporting Information). 15 The corresponding DRIFTS and TGA data for Cs-RHO show a lack of evidence for water desorption by humid CO₂ adsorption (see Figure S7, Supporting Information). We conclude that humid CO2 adsorption in Cs-RHO is consistent with the conventional view on the interactions between CO₂ and water in zeolites, which is encompassed by the longstanding heuristic described above (see Figures S8 and S9 in the Supporting Information). Water isotherm data show that significant pore filling occurs in the RH range of 3-7.5% for Cs-RHO, whereas for K-MER, water uptakes are nearly saturated in this range (see Figure S10, Supporting Information). Based on these data, we surmise that the desorption of water in K-MER cannot be attributed to weaker water adsorption alone. We posit that the observed difference in CO₂ causing no change to the amount of adsorbed water for Cs-RHO versus causing 20.1% water desorption in K-MER is highly sensitive to the local structure of water at the humid CO₂ adsorption site.

To gain more microscopic insight into this possibility, we used DRIFTS to understand the nature of the water that desorbs during humid CO₂ adsorption in K-MER. DRIFTS data show the presence of two different types of adsorbed water in K-MER, which have distinct hydrogen-bonding characteristics (see Figure S11a, Supporting Information).^{30–32} At the lowest background RH (i.e., controlled by the unsealed nature of the TGA equipment and trace amounts of water from the gas cylinders), we see evidence of bulk water clusters with broad hydrogen-bonded water bands with a maximum centered at 3400 cm⁻¹ and a distinct high-energy shoulder at 3561 cm⁻¹. We observe no presence of water species represented by a band at 3612 and 3525 cm⁻¹ at this low RH (see inset in Figure S11a, Supporting Information), but we

do observe these latter bands in K-MER at a higher RH of 5%, along with a concomitant increase in the 3400, 3525, and 3612 cm⁻¹ bands. We also observed the delayed appearance of water species represented by the 3612 and 3525 cm⁻¹ bands in transient water-adsorption experiments (see time-resolved spectra in Figures S12a and S13 in the Supporting Information). Altogether, our data demonstrate that water species represented by bands at 3612 and 3525 cm⁻¹ are distinct species from the more strongly hydrogen-bonded water clusters characteristic of the broad band centered at 3400 cm⁻¹.

On the basis of previous literature, 33-36 we assign the sharp band at 3612 cm⁻¹ to be the -OH stretching vibration of an adsorbed water dimer (i.e., (H₂O)₂) and the 3525 cm⁻¹ band to correspond to slightly more hydrogen-bonded species than this dimer (e.g., (H₂O)₃) in K-MER. 33,36,37 Based on the higher intensity of the 3612 cm⁻¹ band at 5% relative humidity (see Figure S13, Supporting Information), which is known to have a lower extinction coefficient relative to the lower energy species (i.e., band at 3525 cm⁻¹), 31,38 we surmise that the water species represented by the 3612 and 3525 cm⁻¹ bands under our conditions in K-MER mostly represents a water dimer, which is involved in less hydrogen bonding. The DRIFTS data in the inset of Figure 1a demonstrate that the water that desorbed during humid CO2 adsorption in K-MER is represented solely by the 3612 and 3525 cm⁻¹ bands; in particular, the bands for bulk water clusters remain unchanged. Similar DRIFTS data of adsorbed water in Cs-RHO show no evidence of adsorbed dimeric water in this zeolite (see Figures S7 in the Supporting Information). We conclude that CO₂ adsorption causes the desorption of mainly dimeric water within K-MER and that this type of adsorbed water is absent in Cs-RHO. There are a variety of zeolite properties that control these phenomena, such as the framework flexibility and environment surrounding the adsorption site (the D8R diameters and shapes in K-MER and Cs-RHO are subtly different, as are the structures of their cages), which can also be influenced by the cation type and the Si:Al ratio.

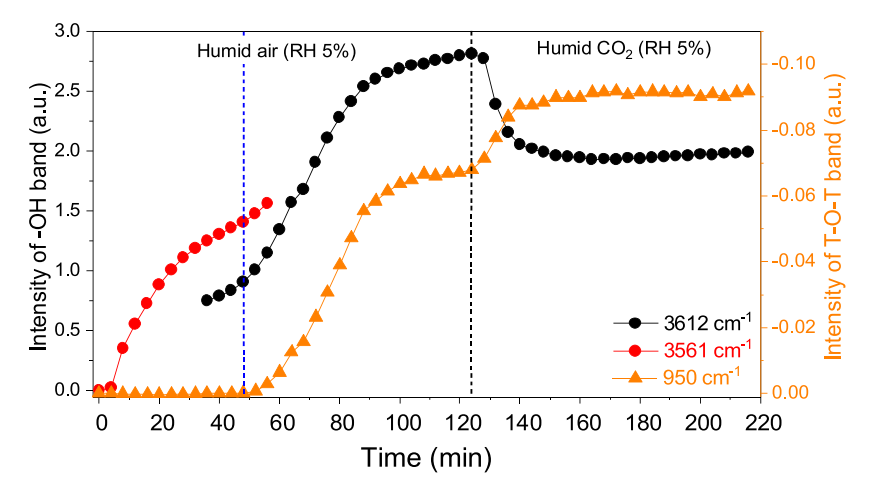


Figure 2. Intensity profiles of infrared bands at 3612, 3561, and 950 cm $^{-1}$ during water adsorption and subsequent humid CO $_2$ adsorption. K-MER is saturated with humid air at 5% RH, 30 $^{\circ}$ C for 120 min. Subsequently humid CO $_2$ adsorption at 5% RH is performed after 124 min (black dashed line) at the same RH and temperature.

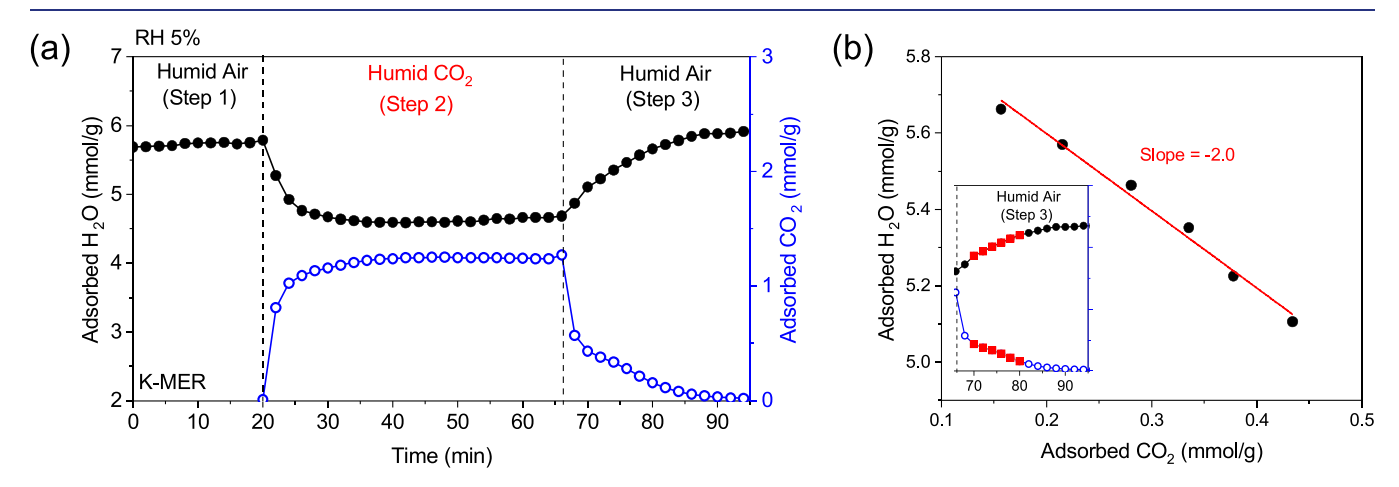


Figure 3. (a) Time-resolved profiles for the amount of adsorbed water and CO_2 in K-MER during humid CO_2 adsorption/desorption at 30 °C under 5% relative humidity. Black circles represent adsorbed water (mmol/g), and blue empty circles represent adsorbed CO_2 (mmol/g). (b) Parametric plot representing the amount of adsorbed water and CO_2 in K-MER during step 3 of Figure 3a. The inset in Figure 3b shows in red the points chosen from Figure 3a.

We investigate how the adsorption of water under equilibrium control influences infrared bands in the T-O-T structural vibrational region (1200-850 cm⁻¹),²⁶ which are perturbed by the cation positions in K-MER. We observe emergence of a strong negative band^{4,39} at 950 cm⁻¹ at 5% RH (see Figure S11b, Supporting Information). This IR band is assigned to asymmetric stretching of perturbed zeolite T-O-T vibrations, which are controlled by cation/framework oxygen (K+-O_f) interactions.³⁹ The negative intensity of this band (relative to dry K-MER zeolite as the background) is a consequence of a weaker K+-O_f interaction upon water adsorption. We infer that the interactions between adsorbed water and K⁺ cations displace the latter from their dry-state equilibrium positions, which are located in the middle of the D8R of K-MER (vide infra). 40 At the lowest background level of RH, we observe no change in the 950 cm⁻¹ band, while we do observe evidence of adsorption of water species represented by the broad band centered at 3400 cm⁻¹ (see Figures S11, Supporting Information).

To gain additional insight, we examined the dynamic intensity profiles for infrared bands at 3612 cm⁻¹ (representing the dimeric water species), 3561 cm⁻¹ (representing the

strongly hydrogen-bound water species characterized by the broad 3400 cm⁻¹-centered band), and 950 cm⁻¹ (representing the framework perturbation band) in time-resolved DRIFTS during water adsorption in K-MER. Figure 2 demonstrates the immediate formation of strongly hydrogen-bound water species and the delayed formation of dimeric water for the first 48 min (blue dashed line) (*vide supra*). Crucially, we observe a perturbation in the 950 cm⁻¹ band only upon adsorption of the dimeric water, but not during the adsorption of the strongly hydrogen-bound water that precedes it (see phase plot in Figure S14, Supporting Information). We infer that it is the dimeric water that uniquely controls the change in the 950 cm⁻¹ band upon K-MER hydration.

In a previous study, water adsorption/desorption in K-MER was characterized by Rietveld refinement of PXRD data, which demonstrates K⁺ migration upon hydration. The most marked change in K⁺ location occurred upon cation migration out of the center of the D8R site (dry equilibrium position), as a result of displacement by adsorbed water occupying this site. Other changes accompanying K-MER hydration such as those involving K⁺ in S8R (single eight-membered ring) sites were more subtle, and we surmise that those changes should have a

smaller effect on the 950 cm $^{-1}$ band. We conclude that the adsorption of dimeric water inside the D8R controls K $^{+}$ -cation migration out of the D8R, and the strongly hydrogen-bound water does not interact with K $^{+}$ in the D8R. Such a confined environment for the dimeric water isolates the water dimer from the more strongly hydrogen-bound water cluster, which is characterized by the broad 3400 cm $^{-1}$ band.

After 120 min of time on stream in Figure 2, we switched the gas from humid air to CO_2 , all while maintaining 5% RH. We observed humid CO_2 adsorption by DRIFTS and tracked the response of the other infrared bands during this adsorption. Dimeric water desorption is observed concomitantly with CO_2 adsorption (i.e., at the black dashed vertical line in Figure 2). At the same time, we observe a slight additional increase in the framework perturbation band at 950 cm $^{-1}$ in Figure 2 (see the raw data in Figure S15 and the phase plot in Figure S16, Supporting Information).

Applying the combined quantification of water and CO₂ with TGA and DRIFTS, Figure 3a shows dynamic profiles for the amount of water and CO2 during adsorption and desorption in K-MER under wet conditions (see raw data in Figure S17, Supporting Information). In step 2 of Figure 3a, we dynamically observe water desorption caused by CO2 adsorption in K-MER. Since water and CO2 compete for the same adsorption site, the CO₂ desorption (shown in step 3 of Figure 3a) causes simultaneous readsorption of water and leads the amount of adsorbed water to ultimately return to its equilibrium level at 5% RH in step 1 of Figure 3a. In Cs-RHO, CO₂ adsorption/desorption under the same conditions does not influence the amount of equilibrated water (see Figures S18 and S19, Supporting Information). Data shown in Figure 3b represent a parametric plot (i.e., where time is implicit) for the relationship between the amount of adsorbed water and CO₂ in K-MER during step 3 in Figures 3a. Based on these data, we clearly see that each CO₂ molecule desorbs two water molecules. Coupling this result to our spectroscopic observations above leads to a single adsorbing CO2 releasing one dimeric water (Figure 1a). Such an outcome is supported by (i) the similar calculated volumes of CO2, a water dimer, and the internal cavity of the D8R in K-MER, as well as (ii) the cumulative molar amount of desorbed dimeric water during CO₂ adsorption being commensurate with the total molar amount of D8R as an upper bound (Figure S20, Supporting Information).

The conclusions demonstrated here highlight the importance of a combined TGA-DRIFTS approach for quantifying humid CO_2 adsorption in zeolites and motivate future mechanistic work aimed at uncovering the controlling features of the selective humid CO_2 binding site described here for K-MER.

ASSOCIATED CONTENT

Data Availability Statement

Data are available from the corresponding authors upon reasonable requests.

Supporting Information

The Supporting Information is available free of charge at https://pubs.acs.org/doi/10.1021/jacs.3c10834.

Experimental details, DRIFT spectra, TGA data (PDF)

AUTHOR INFORMATION

Corresponding Author

Alexander Katz — Department of Chemical and Biomolecular Engineering, University of California, Berkeley, California 94720, United States; orcid.org/0000-0003-3487-7049; Email: askatz@berkeley.edu

Authors

Hwangho Lee – Department of Chemical and Biomolecular Engineering, University of California, Berkeley, California 94720, United States

Dan Xie — Chevron Technology Center, Richmond, California 94801, United States; Present Address: Braskem Renewable Innovation Center, Lexington, Massachusetts 02421, United States

Stacey I. Zones — Chevron Technology Center, Richmond, California 94801, United States; orcid.org/0000-0002-3128-6481

Complete contact information is available at: https://pubs.acs.org/10.1021/jacs.3c10834

Notes

The authors declare no competing financial interest.

ACKNOWLEDGMENTS

The authors gratefully acknowledge funding from the CeRCaS NSF IUCRC for all synthesis aspects related to this work, and DOE, Office of Basic Energy Sciences (DE-FG02-0SER15696), for all aspects covering characterization including by combined TGA and DRIFTS. The authors acknowledge the help of Dave Small at the Berkeley Molecular Computation Graphics Facility, which is funded by NIH S10OD023532, for assistance with calculating molecular volumes.

REFERENCES

- (1) Haszeldine, R. S. Carbon capture and storage: how green can black be? *Science* **2009**, 325 (5948), 1647–1652.
- (2) Fu, D.; Davis, M. E. Carbon dioxide capture with zeotype materials. *Chem. Soc. Rev.* **2022**, *51* (22), 9340–9370.
- (3) Chen, K.; Mousavi, S. H.; Singh, R.; Snurr, R. Q.; Li, G.; Webley, P. A. Gating effect for gas adsorption in microporous materials-mechanisms and applications. *Chem. Soc. Rev.* **2022**, *51* (3), 1139–1166
- (4) Fu, D.; Park, Y.; Davis, M. E. Zinc Containing Small-Pore Zeolites for Capture of Low Concentration Carbon Dioxide. *Angew. Chem., Int. Ed. Engl.* **2022**, *61* (5), No. e202112916.
- (5) Li, G.; Xiao, P.; Webley, P.; Zhang, J.; Singh, R.; Marshall, M. Capture of CO2 from high humidity flue gas by vacuum swing adsorption with zeolite 13X. *Adsorption* **2008**, *14* (2–3), 415–422.
- (6) Sircar, S.; Myers, A. L. Gas separation by zeolites. In *Handbook of Zeolite Science and Technology*; CRC Press, 2003; pp 1354–1406.
- (7) Lozinska, M. M.; Mowat, J. P. S.; Wright, P. A.; Thompson, S. P.; Jorda, J. L.; Palomino, M.; Valencia, S.; Rey, F. Cation Gating and Relocation during the Highly Selective "Trapdoor" Adsorption of CO2 on Univalent Cation Forms of Zeolite Rho. *Chem. Mater.* **2014**, 26 (6), 2052–2061.
- (8) Clatworthy, E. B.; Paecklar, A. A.; Dib, E.; Debost, M.; Barrier, N.; Boullay, P.; Gilson, J.-P.; Nesterenko, N.; Mintova, S. Engineering RHO Nanozeolite: Controlling the Particle Morphology, Al and Cation Content, Stability, and Flexibility. ACS Applied Energy Materials 2022, 5 (5), 6032–6042.
- (9) Choi, H. J.; Jo, D.; Min, J. G.; Hong, S. B. The Origin of Selective Adsorption of CO2 on Merlinoite Zeolites. *Angew. Chem., Int. Ed. Engl.* **2021**, *60* (8), 4307–4314.

- (10) Hudson, M. R.; Queen, W. L.; Mason, J. A.; Fickel, D. W.; Lobo, R. F.; Brown, C. M. Unconventional, highly selective CO2 adsorption in zeolite SSZ-13. *Journal of the American chemical society* **2012**, *134* (4), 1970–1973.
- (11) Shang, J.; Li, G.; Singh, R.; Gu, Q.; Nairn, K. M.; Bastow, T. J.; Medhekar, N.; Doherty, C. M.; Hill, A. J.; Liu, J. Z. Discriminative separation of gases by a "molecular trapdoor" mechanism in chabazite zeolites. *J. Am. Chem. Soc.* **2012**, *134* (46), 19246–19253.
- (12) Georgieva, V. M.; Bruce, E. L.; Verbraeken, M. C.; Scott, A. R.; Casteel, W. J., Jr.; Brandani, S.; Wright, P. A. Triggered Gate Opening and Breathing Effects during Selective CO2 Adsorption by Merlinoite Zeolite. *J. Am. Chem. Soc.* **2019**, *141* (32), 12744–12759.
- (13) Thompson, J. A.; Zones, S. I. Binary- and Pure-Component Adsorption of CO2, H2O, and C6H14 on SSZ-13. *Ind. Eng. Chem. Res.* **2020**, *59* (40), 18151–18159.
- (14) Miyamoto, M.; Ono, S.; Kusukami, K.; Oumi, Y.; Uemiya, S. High Water Tolerance of a Core-Shell-Structured Zeolite for CO2 Adsorptive Separation under Wet Conditions. *ChemSusChem* **2018**, *11* (11), 1756–1760.
- (15) Xu, L.; Okrut, A.; Tate, G. L.; Ohnishi, R.; Wu, K. L.; Xie, D.; Kulkarni, A.; Takewaki, T.; Monnier, J. R.; Katz, A. Cs-RHO Goes from Worst to Best as Water Enhances Equilibrium CO2 Adsorption via Phase Change. *Langmuir* **2021**, *37* (47), 13903–13908.
- (16) Kolle, J. M.; Fayaz, M.; Sayari, A. Understanding the effect of water on CO2 adsorption. Chem. Rev. 2021, 121 (13), 7280-7345.
- (17) Zhou, Y.; Zhang, J.; Wang, L.; Cui, X.; Liu, X.; Wong, S. S.; An, H.; Yan, N.; Xie, J.; Yu, C.; et al. Self-assembled iron-containing mordenite monolith for carbon dioxide sieving. *Science* **2021**, 373 (6552), 315–320.
- (18) Grifoni, E.; Piccini, G.; Lercher, J. A.; Glezakou, V.-A.; Rousseau, R.; Parrinello, M. Confinement effects and acid strength in zeolites. *Nat. Commun.* **2021**, *12* (1), 2630.
- (19) Eckstein, S.; Hintermeier, P. H.; Zhao, R.; Baráth, E.; Shi, H.; Liu, Y.; Lercher, J. A. Influence of hydronium ions in zeolites on sorption. *Angew. Chem., Int. Ed.* **2019**, *58* (11), 3450–3455.
- (20) Sánchez-González, E.; Álvarez, J. R.; Peralta, R. A.; Campos-Reales-Pineda, A.; Tejeda-Cruz, A.; Lima, E.; Balmaseda, J.; González-Zamora, E.; Ibarra, I. A. Water adsorption properties of NOTT-401 and CO2 capture under humid conditions. *ACS omega* **2016**, *1* (2), 305–310.
- (21) Chen, C.; Yang, S.-T.; Ahn, W.-S.; Ryoo, R. Amine-impregnated silica monolith with a hierarchical pore structure: enhancement of CO 2 capture capacity. *Chem. Commun.* **2009**, No. 24, 3627–3629.
- (22) Monazam, E. R.; Breault, R. W.; Fauth, D. J.; Shadle, L. J.; Bayham, S. Insights into the Adsorption of Carbon Dioxide in the Presence of Water Vapor Utilizing a Low Molecular Weight Polyethylenimine-Impregnated CARIACT Silica Sorbent. *Ind. Eng. Chem. Res.* **2017**, *56* (32), 9054–9064.
- (23) Peralta, R. A.; Alcántar-Vázquez, B.; Sánchez-Serratos, M.; González-Zamora, E.; Ibarra, I. A. Carbon dioxide capture in the presence of water vapour in InOF-1. *Inorganic Chemistry Frontiers* **2015**, *2* (10), 898–903.
- (24) Yue, M. B.; Sun, L. B.; Cao, Y.; Wang, Z. J.; Wang, Y.; Yu, Q.; Zhu, J. H. Promoting the CO2 adsorption in the amine-containing SBA-15 by hydroxyl group. *Micropor Mesopor Mat* **2008**, *114* (1–3), 74–81.
- (25) Alvarado-Alvarado, D.; González-Estefan, J. H.; Flores, J. G.; Álvarez, J. R.; Aguilar-Pliego, J.; Islas-Jácome, A.; Chastanet, G.; González-Zamora, E.; Lara-García, H. A.; Alcántar-Vázquez, B. Water adsorption properties of Fe (pz)[Pt (CN) 4] and the capture of CO2 and CO. Organometallics 2020, 39 (7), 949–955.
- (26) Auerbach, S. M.; Carrado, K. A.; Dutta, P. K. Handbook of zeolite science and technology. CRC press: 2003.
- (27) Guo, P.; Shin, J.; Greenaway, A. G.; Min, J. G.; Su, J.; Choi, H. J.; Liu, L.; Cox, P. A.; Hong, S. B.; Wright, P. A. A zeolite family with expanding structural complexity and embedded isoreticular structures. *Nature* **2015**, *524* (7563), 74–78.

- (28) Lozinska, M. M.; Mangano, E.; Mowat, J. P.; Shepherd, A. M.; Howe, R. F.; Thompson, S. P.; Parker, J. E.; Brandani, S.; Wright, P. A. Understanding carbon dioxide adsorption on univalent cation forms of the flexible zeolite Rho at conditions relevant to carbon capture from flue gases. *J. Am. Chem. Soc.* **2012**, *134* (42), 17628–42.
- (29) Xie, D. Potassium-merlinoite zeolite, its synthesis and use. US patent US 11,465,122 B2, October 11, 2022.
- (30) Buckingham, A.; Del Bene, J.; McDowell, S. The hydrogen bond. *Chem. Phys. Lett.* **2008**, 463 (1–3), 1–10.
- (31) Kollman, P. A.; Allen, L. C. Theory of the hydrogen bond. Chem. Rev. 1972, 72 (3), 283-303.
- (32) Bregante, D. T.; Chan, M. C.; Tan, J. Z.; Ayla, E. Z.; Nicholas, C. P.; Shukla, D.; Flaherty, D. W. The shape of water in zeolites and its impact on epoxidation catalysis. *Nature Catalysis* **2021**, *4* (9), 797–808
- (33) Paul, J.; Collier, C.; Saykally, R.; Scherer, J.; O'keefe, A. Direct measurement of water cluster concentrations by infrared cavity ringdown laser absorption spectroscopy. *J. Phys. Chem. A* **1997**, *101* (29), 5211–5214.
- (34) Kondo, J. N.; Iizuka, M.; Domen, K.; Wakabayashi, F. IR study of H2O adsorbed on H-ZSM-5. *Langmuir* **1997**, *13* (4), 747–750.
- (35) Vogt, E.; Kjaergaard, H. G. Vibrational spectroscopy of the water dimer at jet-cooled and atmospheric temperatures. *Annu. Rev. Phys. Chem.* **2022**, *73*, 209–231.
- (36) Buck, U.; Huisken, F. Infrared spectroscopy of size-selected water and methanol clusters. *Chem. Rev.* **2000**, *100* (11), 3863–3890.
- (37) Keutsch, F. N.; Cruzan, J. D.; Saykally, R. J. The water trimer. *Chem. Rev.* **2003**, *103* (7), 2533–2578.
- (38) Van Thiel, M.; Becker, E. D.; Pimentel, G. C. Infrared studies of hydrogen bonding of water by the matrix isolation technique. *J. Chem. Phys.* **1957**, *27* (2), 486–490.
- (39) Kwak, J. H.; Zhu, H.; Lee, J. H.; Peden, C. H.; Szanyi, J. Two different cationic positions in Cu-SSZ-13? *Chem. Commun.* **2012**, 48 (39), 4758–4760.
- (40) Lee, H.; Song, I.; Jeon, S. W.; Kim, D. H. Mobility of Cu Ions in Cu-SSZ-13 Determines the Reactivity of Selective Catalytic Reduction of NOx with NH3. *J. Phys. Chem. Lett.* **2021**, 12 (12), 3210–3216.